

## An adaptive grid version of CMAQ for improving the resolution of plumes

Fernando Garcia–Menendez, Aika Yano, Yongtao Hu, M. Talat Odman

School of Civil and Environmental Engineering, Georgia Institute of Technology, 311 Ferst Drive, Atlanta, GA 30332-0512, USA

### ABSTRACT

Atmospheric pollutant plumes are not well resolved in current air quality models due to limitations in grid resolution. Examples of these include power plant and biomass burning plumes. Adequate resolution of these plumes necessitates multiscale air quality modeling at much finer scales than currently employed and we believe that adaptive grids could be the best approach to accurate fine-scale modeling of air pollution dynamics and chemistry. An adaptive grid version of the CMAQ model with all necessary functions for tracking gaseous pollutants and particulate matter has been developed. The model incorporates a dynamic, solution-adaptive grid algorithm and a variable time step algorithm into CMAQ, while retaining the original functionality, concept of modularity, and grid topology.

The adaptive model was evaluated by comparing its performance to that of the standard, static grid CMAQ in simulating particulate matter concentrations from a biomass burning air pollution incident affecting a large urban area. The adaptive grid model significantly reduced numerical diffusion, produced better defined plumes, and exhibited closer agreement with monitoring site measurements. The adaptive grid also allows impacts at specified locations to be attributed to a specific pollutant source and provides insight into air pollution dynamics unattainable with a static grid model. Potential applications of adaptive grid modeling need not be limited to air quality simulation, but could be useful in meteorological and climate models as well.

### Keywords:

Adaptive mesh refinement  
Modeling of plumes  
Air quality  
Biomass burning  
Particulate matter

### Article History:

Received: 11 April 2010  
Revised: 20 August 2010  
Accepted: 11 September 2010

### Corresponding Author:

M. Talat Odman  
Tel: +1-404-894-2783  
Fax: +1-404-894-8266  
E-mail: talat.odman@ce.gatech.edu

© Author(s) 2010. This work is distributed under the Creative Commons Attribution 3.0 License.

doi: 10.5094/APR.2010.031

### 1. Introduction

The dynamic and chemical processes of air pollution involve a wide range of scales. While the initial transformation of emissions and dispersion of plumes occur on relatively small scales, long-range transport engages much larger scales. Air quality models rely on their grids for explicit resolution of processes involved; the processes that occur on sub-grid scales are parameterized. Modeling large geographic regions with uniform resolution at the finest relevant scale is beyond the realm of current computers; therefore, regional models generally settle for coarser grid resolution. When emissions or plumes are injected into grid cells coarser in size than characteristic plume dimensions, they instantaneously mix with the contents of the grid cell. Such mixing is unrealistic; it dilutes the plumes and the details of the near-field chemistry are lost. Multiscale models have been proposed to surpass the limitations of single scale models. Conceptually, a multiscale model blends small scales with large scales and assigns the most appropriate scales to the phenomenon being modeled.

The approaches to multiscale air quality modeling generally fall into one of the following two categories. The first category features static grids that can be nested multiple levels deep for better resolution of finer scale processes. This is the approach taken in the Community Multiscale Air Quality Model (CMAQ) (Byun and Schere, 2006). The second approach involves grids whose resolutions continuously adapt to the needs of a particular phenomenon throughout the simulation. Note that we did not distinguish sub-grid modeling as a separate category in our classification. Embedding a sub-grid scale model into the grid

model (e.g., plume-in-grid modeling) is a multiscale modeling technique that can be used both with static grid nesting and dynamic grid adaptations.

In static grid nesting, finer grids (FGs) are nested inside coarser ones (CGs). Multilevel nests can be placed to resolve the plumes of interest; however, since wind direction can change during the simulation, there must be fine resolution all around the emission source (e.g., power plant or industrial facility). There are two types of grid nesting: one-way and two-way. In one-way nesting, the CG provides boundary conditions to the FG and no feedback is allowed from the FG to the CG; therefore, the CG and FG can be modeled sequentially. CMAQ uses one-way nesting. In two-way nesting, there is full interaction between the grids and all grids must be modeled simultaneously. The biggest limitation of static grid nesting is that resolution and the extent of each grid must be determined a priori and remain fixed throughout the simulation. One has to make sure that the right choices of scale and coverage are made at the beginning of the simulation.

In dynamic grid adaptations, the grid resolution changes continuously and automatically to improve the ability of the model, to capture detailed dynamics or follow the chemical evolution of plumes. For example, refining the grid where chemical reactivity is high can lead to better characterization of the interactions of pollutant plumes with ambient atmospheres. Similarly, the passage of a front, clouds, and other relevant dynamic features can all be better resolved if dynamic adaptations are used. Dynamic adaptive grids were suggested for use in

atmospheric modeling few decades ago, but did not gain wide-spread acceptance.

Several adaptive grid algorithms were developed specifically for air quality modeling during the last decade. Although these algorithms did not necessarily make their way into functional air quality models, they were quite useful in determining the limitations of alternative approaches. For example, Tomlin et al. (1997; 2000) developed an unstructured grid algorithm for the purpose of resolving pollutant plumes in the boundary layer (Tomlin et al., 1997; Ghorai et al., 2000; Tomlin et al., 2000). This algorithm could have been linked with an adaptive grid meteorology model that also employs unstructured grids (e.g., Bacon et al., 2000) and developed into a transport–chemistry coupled with dynamics modeling system. However, this did not happen. The reason may be the difficulties involved in transferring existing air pollution modeling technologies to unstructured grids. On the other hand, the adaptive grid algorithm developed by Srivastava et al. (2000; 2001a; 2001b) is based on structured grids and may be easier to implement in an air quality modeling system.

Although some adaptive grid air pollution models were developed (e.g., Odman et al., 2001; Odman et al., 2002; Constantinescu et al., 2008), they were limited to gas–phase chemistry. No effort has been reported towards the development of an adaptive grid transport–chemistry model for particulate matter (PM) or the incorporation of any adaptive grid capability into community models. However, dynamic grid adaptations in a community model such as CMAQ can significantly improve modeling, hence the assessment of the air quality impacts, of plumes from specific emission sources, such as power plants or biomass burns.

This paper continues with a description of how an adaptive grid version of the CMAQ model has been developed based on the adaptive grid algorithm by Srivastava et al. (2000) and the adaptive grid air pollution model by Odman et al. (2001). This is followed by a brief account of the model code verification. The adaptive grid version of CMAQ is then applied to the simulation of a biomass burning plume and compared to the standard, static grid version in terms of plume resolution and agreement with ground–level observations.

**2. Model Development Methodology**

The purpose of this work is to obtain more accurate solutions from the CMAQ model for better assessment of the air quality impacts of plumes. The accuracy of the solution of a numerical model can be increased by either using higher order approximations (a.k.a. p–refinement) or by refining the grid. There are two common grid refinement methods: (1) increasing the number of grid elements (h–refinement); and (2) maintaining the same number of grid elements but refining the grid by repositioning the nodes (r–refinement). In adaptive grid refinement, h– or r–, the objective is to generate an optimal grid with available computational resources for the most accurate solution.

The adaptive grid refinement method used here falls into the r–refinement category. It employs a constant number of grid nodes. An important characteristic of the algorithm is that it utilizes a structured grid that partitions a rectangular domain into *N* by *M* quadrilateral cells. The nodes move throughout the simulation but the topology of the grid remains the same. In other words, each node is still connected to the same neighboring nodes and each cell still has the same neighboring cells after the movement. However, the length of the links between nodes and the area of the grid cells change. One advantage of retaining the structure of the grid is that the non–uniform grid in the physical space can be mapped onto a uniform grid in the computational space through a coordinate transformation. The solution of partial differential equations that govern atmospheric diffusion is simpler

on a uniform grid. Another advantage that cannot be achieved by an unstructured grid is compatibility with CMAQ. Not only can the numerical solution schemes developed for CMAQ be used after the coordinate transformation, but the sub–grid parameterizations in CMAQ can be adopted as well (as long as they remain valid within the range of adaptive grid scales). Since these parameterizations assume a certain grid topology, they are generally incompatible with unstructured grids.

The time integration of the governing equations on a dynamic adaptive, i.e. moving, grid can be viewed as a two–step operation. In the first step, *the solution step*, the grid movement is frozen in time and the equations are solved on this stationary grid. In the second step, *the adaptation step*, the grid nodes are moved through the solution, i.e. concentration, fields obtained in the first step. As a result of the movement of the grid nodes to new locations, it will appear as if fluxes are crossing the faces of the grid cells. Ideally, the adaptation step should be repeated after each solution step owing to the change in resolution requirements. However, since frequent adaptations may be computationally restrictive, we have chosen to apply the adaptation step less frequently than the solution step. A logical choice was to perform grid adaptation once every output time step as, in CMAQ, the partial solutions for different processes are guaranteed to synchronize before the solution is outputted. However, considering that an hour, the typical output time step in CMAQ, may be too long without any adaptation, the output time step was reduced to 15 minutes.

Development of the adaptive grid CMAQ (AG–CMAQ) involved four major tasks: (1) reformulation of governing equations in general curvilinear coordinates; (2) implementation of spatially varying time steps; (3) incorporation of the adaptive grid algorithm; and, (4) consideration of meteorological data and emissions. The first two tasks are related to the solution step. The third and fourth tasks belong to the adaptation step. These four tasks will be described next. The section will end with a brief account of the code verification procedure.

**2.1. Governing equations and coordinate transformation**

CMAQ is based on the species continuity equation that relates the rate of change of the concentration of species *n*, *c<sub>n</sub>*, to transport and chemistry as follows:

$$\frac{\partial(\gamma c_n)}{\partial t} + \frac{\partial(\gamma U c_n)}{\partial X} + \frac{\partial(\gamma V c_n)}{\partial Y} + \frac{\partial(\gamma \dot{\sigma} c_n)}{\partial \sigma} + \frac{\partial}{\partial X} \left( \gamma K^{xx} \frac{\partial c_n}{\partial X} \right) + \frac{\partial}{\partial Y} \left( \gamma K^{yy} \frac{\partial c_n}{\partial Y} \right) + \frac{\partial}{\partial \sigma} \left( \gamma K^{\sigma\sigma} \frac{\partial c_n}{\partial \sigma} \right) = \gamma R_n + \gamma S_n \tag{1}$$

where *X* and *Y* are the coordinates on a conformal map of Earth and  $\sigma$  is a terrain–following normalized vertical coordinate. Hence, the spherical shape of Earth and the irregularity of its surface already necessitated coordinate transformations, and  $\gamma$  is the Jacobian of these transformations:

$$\gamma = \frac{1}{m^2} \frac{\partial z}{\partial \sigma} \tag{2}$$

Here *m* is the scale factor of a conformal map projection, i.e., the ratio of the distance on map to distance on Earth. A popular normalized vertical coordinate is sigma–p (pressure) which is related to the altitude coordinate *z* as  $\partial z / \partial \sigma = p^* / \rho g$ , where *p\** is the pressure difference between the surface and the top of the domain,  $\rho$  is the air density, and *g* is the gravitational acceleration. In Equation (1), *U* and *V* are the wind velocity components in the *X* and *Y* directions after scaling by *m*, and  $\dot{\sigma}$  is a non–dimensional velocity component in the  $\sigma$  direction.  $K^{xx}$ ,

$K^{yy}$  and  $K^{\sigma\sigma}$  are the elements of the diagonal turbulent diffusivity tensor with  $K^{\sigma\sigma}$  related to vertical diffusivity  $K^{zz}$  as:

$$K^{\sigma\sigma} = \left( \frac{\partial \sigma}{\partial z} \right)^2 K^{zz} \quad (3)$$

$R_n$  and  $S_n$  are the chemical reaction and emission terms for species  $n$ . There are also terms related to aerosol and cloud processes in CMAQ, but they are not shown here for simplicity.

One more coordinate transformation was necessary to develop AG-CMAQ, and that is the transformation of the horizontal space from the  $(X, Y)$  coordinate system to a curvilinear coordinate system  $(\xi, \eta)$ :

$$\begin{aligned} \xi &= \xi(X, Y) \\ \eta &= \eta(X, Y) \end{aligned} \quad (4)$$

Through this transformation, the adaptive grid that is non-uniform in  $(X, Y)$  space becomes a uniform grid in  $(\xi, \eta)$  space. The governing equations in  $(\xi, \eta, \sigma)$  space can be derived from Equation (1) above through the use of the chain rule for derivatives:

$$\begin{aligned} \frac{\partial (Jc_n)}{\partial t} + \frac{\partial (Jv^\xi c_n)}{\partial \xi} + \frac{\partial (Jv^\eta c_n)}{\partial \eta} + \frac{\partial (J\sigma c_n)}{\partial \sigma} + \frac{\partial}{\partial \xi} \left( JK^{\xi\xi} \frac{\partial c_n}{\partial \xi} \right) \\ + \frac{\partial}{\partial \eta} \left( JK^{\eta\eta} \frac{\partial c_n}{\partial \eta} \right) + \frac{\partial}{\partial \sigma} \left( JK^{\sigma\sigma} \frac{\partial c_n}{\partial \sigma} \right) = JR_n + JS_n \end{aligned} \quad (5)$$

In this equation, the new Jacobian,  $J$ , is related to  $\gamma$  as:

$$J = \left( \frac{\partial X}{\partial \xi} \frac{\partial Y}{\partial \eta} - \frac{\partial Y}{\partial \xi} \frac{\partial X}{\partial \eta} \right) \gamma \quad (6)$$

and  $v^\xi$  and  $v^\eta$  are the non-dimensional components of the wind velocity vector in the  $\xi$  and  $\eta$  directions related to  $U$  and  $V$  as:

$$\begin{aligned} v^\xi &= \frac{\partial \xi}{\partial X} U + \frac{\partial \xi}{\partial Y} V \\ v^\eta &= \frac{\partial \eta}{\partial X} U + \frac{\partial \eta}{\partial Y} V \end{aligned} \quad (7)$$

The expressions for the elements of the turbulent diffusivity tensor  $K^{\xi\xi}$ ,  $K^{\eta\eta}$  are rather long and they will not be included here.

Now that the grid is uniform in  $(\xi, \eta)$  space, it is much easier to solve the Equation (5). In fact, since the finite difference stencils in the  $\xi$  and  $\eta$  directions are the same as the stencils used in the  $X$  and  $Y$  directions in CMAQ, the solution algorithms can be taken directly from CMAQ. In addition, the parameterizations that only involve the vertical direction (e.g., cumulus parameterization) are directly applicable since we did not transform the vertical coordinate. The metric derivatives in Equations (6) and (7) are calculated after each grid adaptation step using finite differences at the most appropriate locations (i.e., at the grid nodes or at the centers of the grid cells), stored as global variables, and then passed to various process modules that need them.

## 2.2. Variable time-step algorithm

In CMAQ, Equation (1) is solved using a method called process splitting where the rate of change of concentrations in one time step is broken into components associated with each process. These processes (i.e., advection, diffusion, and chemistry, as well as the aerosol and cloud processes) not shown in Equation (1), are

applied to the concentration fields sequentially. After all the processes are applied for one time step, the solution is complete. The time step used for advancing split processes in CMAQ is determined by the characteristic time for advection. The goal is to complete the process cycle before any material is advected by more than one grid cell distance. This is ensured by selecting a time step less than the grid size divided by the wind speed. This also satisfies the Courant stability condition for explicit advection schemes. Since the grid size is uniform in CMAQ, the maximum wind speed determines the time step for the entire domain. Note that using a time step much smaller than a cell's characteristic time step does not make the solution more accurate; therefore, having a single global time step is computationally inefficient. In AG-CMAQ, the grid size is not uniform and the minimum ratio of grid size to wind speed (i.e. a relatively small grid size and a relatively large wind speed) determines the time step. Since the smallest and largest grid sizes can differ by orders of magnitude, the inefficiency becomes a serious bottleneck. Odman and Hu (2007) developed an algorithm that overcomes the global time step limitation by allowing the use of local time steps.

In the variable time step algorithm, VARTSTEP (Odman and Hu, 2010), every cell is assigned its own local time step, which must be an integer multiple of the smallest time step in the domain and a whole divisor of the model's output time step. For example, if the smallest time step in the domain is 1 minute and the output time step is 15 minutes, the allowable local time steps are 1, 3, 5, and 15 minutes. Considering that the length scales may be as small as 10 m in AG-CMAQ, and with a 10 m s<sup>-1</sup> wind speed a time step of 1 s may be necessary, the lower bound for local time steps was decreased to 1 second. With this adjustment, there is now a much wider range of possible local time steps than in the above example. The model clock time,  $t$ , is advanced by the minimum time step in the domain. When the clock strikes a multiple of the local time step, the grid concentration is advanced by the local time step by applying the changes resulting from different processes.

Greatest computational savings can be expected in chemistry and aerosol processes that are independent from neighboring cell concentrations because the changes due to those processes can be computed at the frequency of the local time steps. On the other hand, transport processes involve neighboring cell concentrations; therefore, they must be computed more frequently than the local time step. The transport fluxes from neighboring cells must be kept in reservoirs until the concentrations are updated. This increases the memory requirements with respect to CMAQ by an array equal in size to the concentration array. Horizontal advection in all grid cells is computed at the frequency of the minimum time step in the domain. Chemistry and aerosol processes are computationally more intensive than horizontal advection in CMAQ (Odman and Hu, 2010). As a result, the local time stepping enabled by VARTSTEP makes AG-CMAQ much more computationally efficient than its predecessors (Odman et al., 2001; Odman et al., 2002).

## 2.3. Adaptive grid algorithm

As mentioned before, a simulation with AG-CMAQ has two fundamental steps: the solution step, as described above, and the grid adaptation step that will be described here. The purpose of grid adaptation is to locally increase or decrease grid resolution such that a more accurate solution can be obtained in the following solution step. The solution (i.e., concentration) fields remain unchanged during the adaptation step. The grid nodes are clustered in regions where finer resolution is needed for an accurate solution.

The grid adaptation methodology used here is based on the Dynamic Solution Adaptive Grid Algorithm (DSAGA) described in Srivastava et al. (2000). In this algorithm, the movement of the grid nodes is controlled by a weight function. The grid resolution is increased by clustering the grid nodes around regions where the

weight function bears large values. Since the number of nodes is constant, refinement of the grid in some regions of the domain is accompanied by coarsening in other regions where the weight function has smaller values. In this manner, a multiscale grid is obtained where the scales change gradually. Unlike nested grids, there are no fine-to-coarse grid interfaces, which may introduce numerical difficulties due to the abrupt change (i.e. discontinuity) of grid scales. In practice, the number of grid nodes is selected according to the computational resources available. By distributing the grid nodes automatically throughout the modeling domain, DSAGA makes optimal use of computational resources throughout the simulation.

The weight function must be able to determine where grid nodes are to be clustered for a more accurate solution. A linear combination of the errors in concentrations of various chemical species makes an ideal weight function because it will assume large values where the errors are large:

$$w = \sum_n \alpha_n \nabla^2 c_n \quad (8)$$

where  $w$  is the weight function;  $\nabla^2$ , the Laplacian, is a measure for the numerical error in  $C_n$  and  $\alpha_n$  is a coefficient that adjusts the weight of the numerical error in species  $n$  with respect to the others. The different chemical mechanisms used in CMAQ all have a large number of species. Each one of these species may have very different resolution requirements. Therefore, no single set of  $\alpha_n$  can guarantee accurate solutions for all applications. In what follows, the focus was on PM emissions from biomass burning; therefore, all  $\alpha_n$  were set to zero, except for those of primary PM species. In applications involving secondary pollutants (e.g., ozone or secondary organic aerosols) the proper choice of  $\alpha_n$  may not be as obvious and may require some experimentation. For example, a weight function combining nitrogen oxides ( $\text{NO}_x$ ), volatile organic compounds (VOCs) and ozone is likely to produce the best grid for capturing ozone formation. Odman et al. (2002), Khan (2003), and Constantinescu et al. (2008) tried weight functions with different combinations of  $\alpha_n$  for  $\text{NO}_x$ , VOC, and ozone, in applications to urban and power plant plumes.

The current grid adaptation in AG-CMAQ is in the horizontal plane only, i.e., the resulting grid is the same in all vertical layers. Therefore, surface or any other layer concentrations, or vertical column totals may be used in Equation (8). Using the weight function, the new position of the grid node  $i$ ,  $\bar{P}_i^{new}$ , is calculated as follows:

$$\bar{P}_i^{new} = \frac{\sum_{k=1}^4 w_k \bar{P}_k}{\sum_{k=1}^4 w_k} \quad (9)$$

Here,  $\bar{P}_k$ ,  $k=1, \dots, 4$  are the original positions of the centroids of four grid cells that share the grid node  $i$  in the horizontal plane, and  $w_k$  is the value of the weight function at each centroid. Although only  $X$  and  $Y$  change and  $\sigma$  remains the same after adaptation, the grid node coordinates  $(X, Y, \sigma)$  were stored in a 3-D array,  $XGRID$ , to allow for vertical adaptation in the future.  $XGRID$  is passed as an argument to all of the process modules.

The movement of grid nodes in a steady concentration field results in fluxes crossing the boundaries of the grid cells. In this respect, grid adaptation is similar to advection where the grid boundaries are fixed but the field is moving due to wind velocity. Another way of attacking the problem is to observe that after the grid adaptation each grid cell encloses a different portion of the domain, hence a different plot of the concentration field. Therefore, cell-average concentrations must be recomputed. This is more similar to interpolation. Since interpolation is numerically equivalent to advection (Smolarkiewicz and Grell, 1992), either

way of thinking is acceptable. We used a high-order accurate and monotonic advection scheme known as the piecewise parabolic method (Colella and Woodward, 1984) to determine the concentrations of grid cells after adaptation.

Grid adaptation is an iterative process that continues until the optimal grid is found. Note that the concentration field must be redistributed (i.e., interpolated as described above using the advection scheme) to the new grid locations and the weight function must be recalculated at every iteration. The grid is considered to have converged when the new positions in Equation (9) are the same, i.e., within a preset tolerance, as the old positions. A very small tolerance may lead to a large number of iterations. On the other hand, a large tolerance may not yield adequate grid resolution for minimizing the numerical error in concentrations. After rigorous testing with alternative values of the tolerance, we decided to stop iterating when, for any grid node, the movement is less than 5% of the minimum distance between the node in question and the four nodes to which it is connected in the horizontal plane.

#### 2.4. Meteorological data and emissions

After the grid adaptation, meteorological data and emissions are needed on the new grid locations for the next solution step. For meteorological data, an ideal solution would be to have a meteorological model that can operate on the same adaptive grid and run in parallel with AG-CMAQ. The weight function that drives grid adaptations can include functions of meteorological variables such as vorticity. Such an adaptive grid meteorological model can also resolve local circulations that cannot be detected by static grid meteorological models, even at very fine (e.g., 1-km) grid resolutions. Recently, an adaptive grid version of the MM5 numerical weather prediction model was developed based on DSAGA for the purpose of predicting optical turbulence in the upper atmosphere (Xiao et al., 2006). However, at the time of the present study, that model was still under evaluation for applications within the boundary layer. In the absence of an adaptive grid meteorology model, the best available option was to obtain the data from a high-resolution, static-grid meteorological model, store it in a uniform grid input file at 15-minute frequency and, when needed in AG-CMAQ, interpolate onto the adaptive grid. The interpolation weights were calculated after each grid adaptation step and stored as global variables, in the same manner as the metric derivatives.

The processing of emissions is computationally expensive, requiring relocation of various emission sources in the adapted grid cells. Khan et al. (2005) developed efficient search and intersection algorithms for emissions processing. Here, we treated all emissions either as foreground or background emissions. For example, if AG-CMAQ is being used to resolve a biomass burning plume, the emissions from that burn are considered to be in the foreground, while all other emissions (e.g., power plant, industrial, traffic, and biogenic emissions) are in the background. If the foreground emissions are from a stack (e.g., a power plant), the position of the stack must be relocated on the grid as the cell containing the stack may have changed after grid adaptations. If the foreground emissions are from an area source (e.g. a forest fire) then the area of the source must be intersected with the adaptive grid. Since the focus is usually on a few foreground sources, these search and intersection operations are not very intensive. In order to avoid higher computational costs associated with processing of emissions, background emissions are all merged and mapped onto a uniform high-resolution *emissions grid*. Each adaptive grid cell intersects with a number of emissions grid cells. The polygonal intersections of emissions grid cells with adaptive grid cells are calculated and stored as global variables after the grid adaptation step. When emissions are needed during the solution step, the fluxes are read from the emissions input file and apportioned to

the adaptive grid cells using these polygonal intersections as described in Odman et al. (2002).

### 2.5. Code verification

The development of AG-CMAQ was a major undertaking. In addition to adding the adaptive grid related modules, important modifications had to be made to the base CMAQ code; however, special care was taken to remain faithful to the original modularity concept. Several rounds of code reviews were conducted by at least two authors critically examining the code together and making sure that it reflects the intent of the methodology. As a side benefit of these reviews, a few deeply hidden bugs were discovered in the base CMAQ code (see "Bug Alerts" under <http://people.ce.gatech.edu/~odman>). Finally, carefully designed tests were executed to complete the verification of the AG-CMAQ code.

Two of those code verification tests were most useful. In the first test, results from a standard, static-grid CMAQ simulation were compared to those obtained from AG-CMAQ without activating any grid adaptation. The measure of success in this test would be the similarity of results from the newly developed code to the benchmark. Emission data and model inputs corresponding to a controlled forest fire performed at Ft. Benning, Georgia on April 9, 2008 were used in the simulations. The results from the application of AG-CMAQ without adaptation were practically the same to those from the static grid CMAQ, except for very small and random differences, mostly in biogenic organic and nitrate aerosol concentrations ( $< 0.1 \mu\text{g m}^{-3}$ ). A second verification test was carried out to observe the performance of AG-CMAQ with grid adaptation in the simulation of the same controlled forest fire. In this test, to refine the grid around the fire plume in AG-CMAQ, fine particulate matter ( $\text{PM}_{2.5}$ ) concentration was used as the adaptation variable. Modeled surface-level  $\text{PM}_{2.5}$  concentration fields are shown in Figure 1. The results from AG-CMAQ were as expected: grid resolution was increased in the regions of highest  $\text{PM}_{2.5}$  concentration. In the area of highest resolution, grid cell size was reduced down to approximately  $100 \text{ m} \times 100 \text{ m}$  from the initial grid dimensions of  $1.3 \text{ km} \times 1.3 \text{ km}$ . A reduction in the artificial dispersion of the plume, typical of photochemical models, was also evident from the simulation.

## 3. Model Evaluation Results and Discussion

In previous studies, the adaptive grid algorithm was evaluated using problems with increasing complexity and relevance to air quality modeling. Starting with pure advection tests (Srivastava et

al., 2000), idealized reactive flow (Srivastava et al., 2001a) and plume dispersion cases (Srivastava et al., 2001b) were simulated using DSAGA. The performance of the algorithm in tracking multiple urban and power plant plumes was also demonstrated (Khan et al., 2005). In all these applications, the adaptive grid solution was more accurate than the static, uniform grid solution with the same number of grid nodes. Here, the algorithm will be evaluated in AG-CMAQ by a regional-scale air quality simulation that involves a biomass burning event.

In the U.S., controlled forest fires, or prescribed burns, are successfully applied as a land management strategy. Prescribed burns are commonly carried out throughout the Southeastern U.S. and have proven to be effective towards accomplishing different objectives such as habitat restoration, wildfire prevention, endangered species protection, site preparation for seeding and planting, disease control, and appearance enhancement, among others. However, pollutants emitted from prescribed burns may be transported and react to form other pollutants, contributing to poor air quality in downwind urban areas. In the Southeastern U.S., prescribed burns are an important source of primary  $\text{PM}_{2.5}$  and gaseous pollutants. One study found that in this region forest fires account for approximately 20% of  $\text{PM}_{2.5}$  emissions, 8% of carbon monoxide emissions, and 6% of organic compound emissions (Lee et al., 2005).

Air pollution episodes caused by prescribed burning are excellent examples of highly concentrated events occurring at a finer, local scale with an impact that transitions into a larger, regional scale downwind. Prescribed burn plume development typically occurs at scales below those suitable for existing photochemical models due to limitations in grid resolution. In this initial evaluation of AG-CMAQ performance, we analyzed the simulation of a large prescribed burn incident affecting a large urban area. However, AG-CMAQ can be applied to any type of pollution plume and is not limited to those resulting from prescribed burns or forest fires. Our evaluation compares the performance of AG-CMAQ and a standard static grid version of CMAQ. Differences in the simulation results were determined from surface level pollutant concentrations and 3-dimensional visualizations of modeled plumes. Additionally, modeled concentrations are compared to measurements from 6 monitoring stations impacted by the analyzed smoke incident.

### 3.1. Application

On 28 February 2007, air quality in the Atlanta metropolitan area was impacted by heavy smoke caused by prescribed burns.

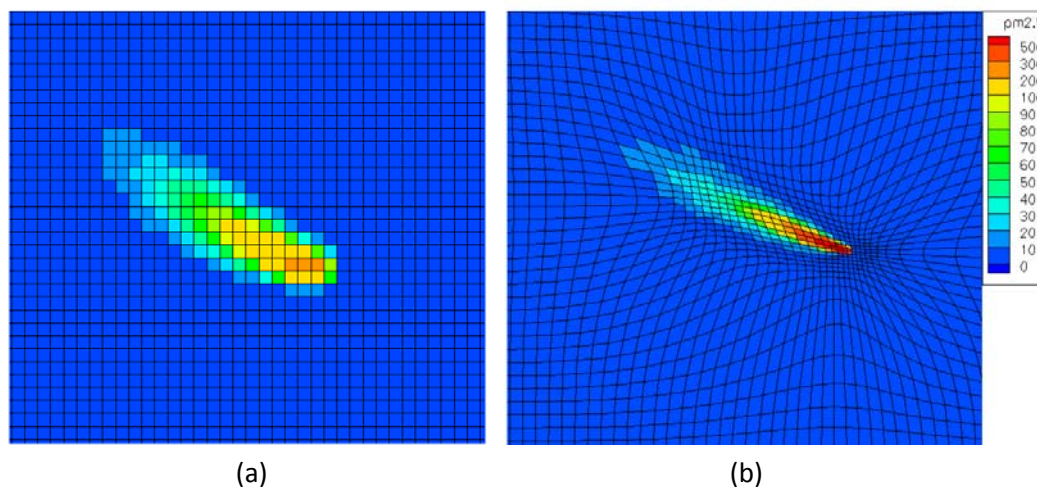


**Figure 1.** Comparison of  $\text{PM}_{2.5}$  concentrations ( $\mu\text{g m}^{-3}$ ) at Fort Benning, Georgia (U.S.A.) during a prescribed burn on 8 April 2008: **(a)** standard CMAQ with 1.33 km grid resolution, **(b)** adaptive CMAQ with dynamically adapting mesh. This figure was originally published in 'Air Pollution Modeling and its Application XX', D.G. Steyn, S.T. Rao, Springer Science + Business Media, 2010, p. 191.

Within hours,  $PM_{2.5}$  levels at monitoring sites throughout the area increased to nearly  $150 \mu\text{g m}^{-3}$  and ozone levels exhibited increments as large as 30 ppb (Hu et al., 2008). Although several prescribed burns were carried out throughout the day, the dramatic increase in pollution levels is mainly attributed to 2 prescribed burns 80 km southeast of Atlanta, one in the Oconee National Forest and another in Piedmont National Wildlife Refuge. In these burns, about  $12 \text{ km}^2$  of land were subjected to treatment. Simulation of the 28 February Atlanta smoke episode with CMAQ at 4-km resolution has been previously carried out and is discussed in Hu et al. (2008). Though the predicted hourly maximum  $PM_{2.5}$  in the Atlanta metropolitan area followed a trend similar to the observed hourly maximum  $PM_{2.5}$  in the area, the simulation failed to place the plume in the right place at the right time. Since the smoke from prescribed burns was detected at multiple local monitoring sites, this event provides a unique opportunity to evaluate AG-CMAQ and compare its performance to standard CMAQ.

In this study, we used the Weather Research and Forecasting model (WRF, version 2.2) (Michalakes et al., 2005) for meteorology and the Sparse Matrix Operator Kernel Emissions model (SMOKE, version 2.1) (Coats, 1996) for emissions other than biomass burning. The WRF simulation started from a 12-km grid over the South-eastern U.S. and nested down to the 4-km grid over Georgia. Analysis products from the North American Mesoscale (NAM) model (nomads.ncdc.noaa.gov) were utilized to initialize WRF, constrain boundary conditions, and nudge simulated fields at 6-h intervals. The emission inventory used as input to SMOKE is projected from a 2002 “typical year” inventory developed for Southeastern U.S. (MACTEC, 2008). The biomass burning emissions were estimated by the Fire Emission Production Simulator (FEPS) (Sandberg et al., 2005) using the information collected and prepared after the burns (Hu et al., 2008). This information includes the actual area burned each hour, fuel moisture, fuel consumption estimated using the Consume 3.0 model (<http://www.fs.fed.us/pnw/fera/research/smoke/consume/index.shtml>), and hourly combustion phase (flaming or smoldering) information. We also used local meteorology and plume temperature data to estimate plume rise and vertical plume profile with Daysmoke, a plume-rise model specifically developed for prescribed burns (Liu et al., 2008). The number of updraft cores, which is an important parameter in Daysmoke, was set to 6 despite the large area of the burns, primarily because of the mass ignition techniques employed and hot burning temperatures; both of these factors should organize the plume in fewer updraft cores. Burn emissions were then injected into CMAQ grid cells, according to their horizontal position with respect to the burn area and, vertically, using the estimated hourly layer-fraction information. At the hour when burn emissions peaked, about 75% of the plume fell into layer 8 of CMAQ (out of 13 total), between 1 090 and 1 865 m above the ground.

### 3.2. Results

The simulation was initiated at 21:00 Z on 27 February and finalized at 05:00 Z on 1 March. Grid adaptation commenced at 15:00 Z on 28 February consistent with initial emissions from the Oconee National Forest and Piedmont National Wildlife Refuge fires. Grid refinement in AG-CMAQ was driven by  $PM_{2.5}$  concentrations. Figure 2 shows  $PM_{2.5}$  concentrations on the modeling domain at 04:45 Z on 1 March after full plume development from both the AG-CMAQ and standard CMAQ simulations. Visual inspection of the modeled  $PM_{2.5}$  surface level concentration fields provides evidence of significant differences between the adaptive grid and static grid simulations. The artificial dilution effect commonly present in gridded photochemical models appears to decrease when applying an adaptive grid. The smoke plumes drawn with AG-CMAQ appear better defined and pollutant concentrations remain higher near plume cores. Most significantly

perhaps, plumes from the two different ongoing prescribed burns can be distinctly observed when applying an adaptive grid. By using a static grid, the plumes cannot be distinguished from each other and appear as a single thicker plume. We believe that in this case the results from AG-CMAQ allow for a better understanding of changes to local air quality and pollutant dispersion.

Analysis of simulated results was extended beyond surface layer concentrations to include pollutant concentrations and plume dynamics aloft. Figure 3 shows a three-dimensional (3D) plot of  $PM_{2.5}$  concentrations which includes concentrations at the surface level and domain boundaries, as well as the 3D pollutant plume defined as a constant concentration surface for concentrations greater than  $50 \mu\text{g m}^{-3}$ . The tops of the plots face the North-western corner of the domain with plumes blowing in the direction of Atlanta. A comparison of the results produced by CMAQ and AG-CMAQ with the use of 3D visualizations provides insight into differences between the simulations not evident from simple surface-level concentration fields. Two differences between both model simulations are most striking. As was observed from the surface-level concentrations plots, the plumes from both targeted ongoing prescribed burns are undistinguishable and appear as a single merged plume using CMAQ results. However, the results from AG-CMAQ allow plumes from both prescribed burns to be distinctly observed. Unlike the static grid simulation, AG-CMAQ allows impacts from smoke plumes at specified locations to be attributed to a specific prescribed burn. It is also apparent that with the static grid simulation a significant portion of the smoke plume initially bifurcates from the main body of the plume directed towards Atlanta due to upper-level wind shear and heads north at a higher altitude (Figure 3a). This bifurcation is not perceived from surface-level concentration fields and more importantly is not present in the AG-CMAQ simulation. The detachment of a plume fragment could partially explain CMAQ's under-prediction of pollutant concentrations at monitoring sites.

Modeled concentrations from both static grid CMAQ and AG-CMAQ simulations were compared to concentration measurements at several air quality monitoring sites in the Atlanta metropolitan area that experienced a significant increase in  $PM_{2.5}$  concentrations during the event. Results from both simulations are plotted along with hourly measurements at six monitoring sites in Figure 4. All sites are concentrated around the city of Atlanta with exception of the McDonough monitoring station located about 40 km away, halfway between the city of Atlanta and the location of the prescribed burns. The tendencies of modeled and observed concentrations at the sites considered are generally similar among each other with exception of the McDonough site. At all sites excluding McDonough, results from the static grid CMAQ simulation consistently under-predict maximum  $PM_{2.5}$  concentrations by 58–70% of measured values. Additionally, the CMAQ results at these sites exhibit two distinct concentration peaks unlike the monitoring station observations. The simulation with AG-CMAQ results in higher concentration maximums at all locations, with exception of the McDonough site, by 27–40% relative to static grid CMAQ maximum concentrations.

The significance of the double peak behavior observed with the static grid results is lessened using AG-CMAQ as results show a more prominent concentration increase at a single major concentration spike. However, a delay of approximately 1 hour in concentration peaks is observed in the AG-CMAQ simulation with respect to static grid CMAQ results which exhibits timing more consistent with monitoring station measurements. Table 1 presents a statistical comparison of model error for CMAQ and AG-CMAQ relative to monitoring station measurements.

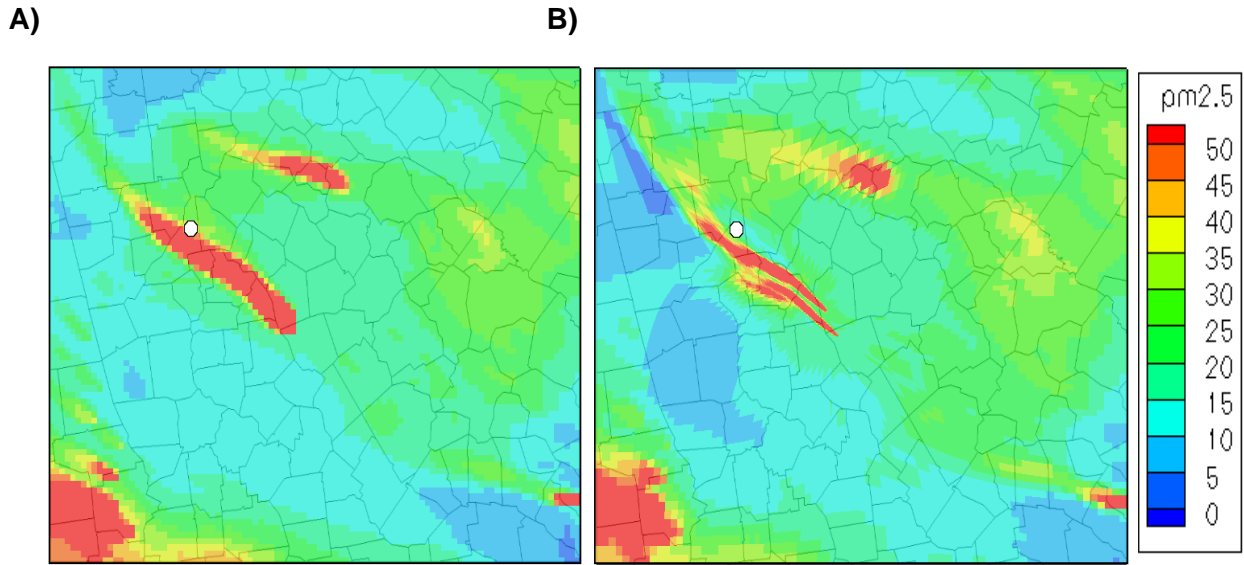


Figure 2. Simulated PM<sub>2.5</sub> concentrations ( $\mu\text{g m}^{-3}$ ) in the surface layer over Georgia, U.S.A. at 04:45 Z on 1 March 2007 using A) static grid CMAQ and B) AG-CMAQ. The location of Atlanta is denoted by a white circle.

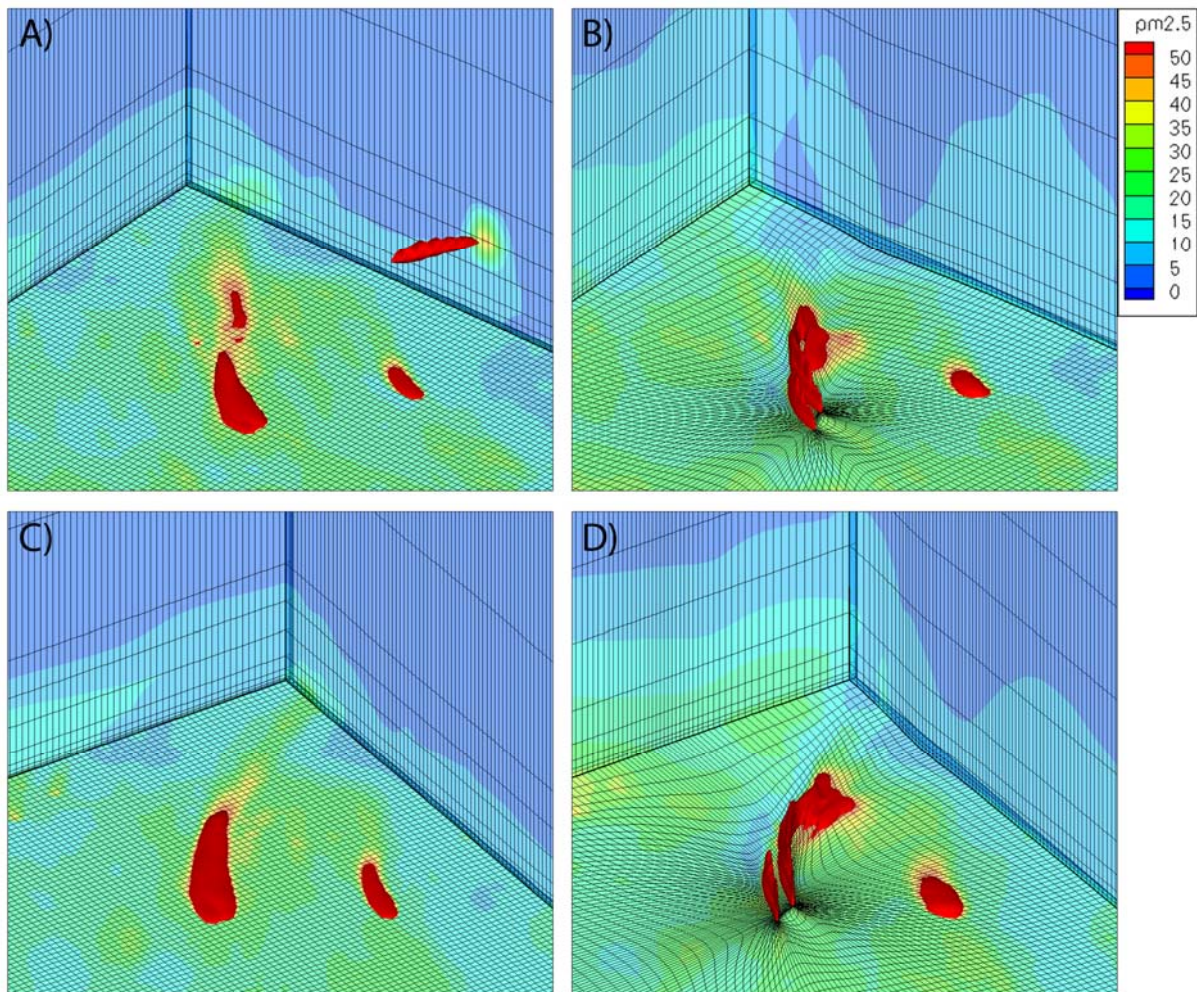


Figure 3. Three-dimensional visualization of smoke plumes and PM<sub>2.5</sub> concentrations ( $\mu\text{g m}^{-3}$ ) on 1 March 2007 at 0:30 Z using A) static grid CMAQ and B) AG-CMAQ, and at 2:15 Z using C) static grid CMAQ and D) AG-CMAQ.

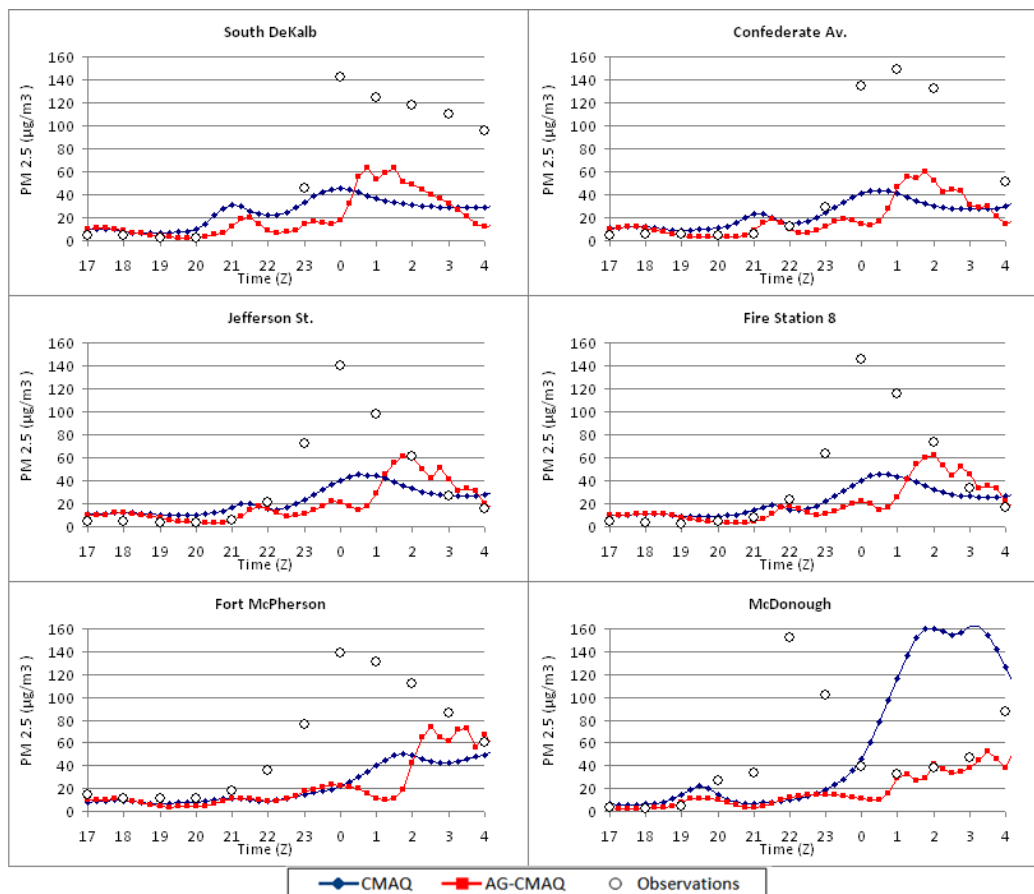


Figure 4. Modeled  $PM_{2.5}$  concentrations ( $\mu g m^{-3}$ ) using static grid CMAQ and AG–CMAQ along with concentration measurements at the South DeKalb, Confederate Avenue, Jefferson Street, Fire Station8, Fort McPherson, and McDonough air quality monitoring sites in the Atlanta metropolitan area.

Table 1. Model error metrics for CMAQ and AG–CMAQ relative to  $PM_{2.5}$  observations at the Jefferson Street (JST), Confederate Avenue (CFA), McDonough (MCD), South DeKalb (SDK), Fort McPherson (FTM), and Fire Station 8 (FS8) monitoring sites and their averages (Avg.)

	Mean Error ( $\mu g/m^3$ ) <sup>a</sup>		Mean Normalized Error (%)		Normalized Mean Error (%)		Mean Fractional Error (%)	
	CMAQ	AG-CMAQ	CMAQ	AG-CMAQ	CMAQ	AG-CMAQ	CMAQ	AG-CMAQ
JST	21.9	21.7	114.1	71.4	65.4	65.0	78.0	58.3
CFA	28.9	29.4	82.8	57.0	66.4	67.5	66.5	58.3
MCD	47.2	27.6	131.3	58.6	111.8	65.3	92.5	64.3
SDK	39.0	40.5	94.9	70.1	68.5	71.0	85.7	78.6
FTM	32.2	33.3	48.6	52.3	60.6	62.7	69.7	74.4
FS8	23.2	23.8	97.0	83.4	63.8	65.4	72.5	65.0
<b>Avg.</b>	<b>32.1</b>	<b>29.4</b>	<b>94.8</b>	<b>65.5</b>	<b>72.7</b>	<b>66.2</b>	<b>77.5</b>	<b>66.5</b>

<sup>a</sup> Modeled concentration (m), observed concentration (o), Number of modeled/observed concentration pairs (N)

A closer look at the surface-level concentration fields along with the location of the six monitoring sites can explain some of the features observed on the time series plots. Four of the sites, South Dekalb, Confederate Av., Jefferson St., and Fire Station 8, are located in this order along a straight path downwind of the prescribed burns. Correspondingly, all increases in  $PM_{2.5}$  concentrations recorded for these sites occur following the same timing pattern from the station closest to the prescribed burns to the furthest. Figure 5a shows surface-level concentrations and monitoring site locations from the static grid simulation at 22:30 Z on 28 February. The simulated plume appears fragmented into two segments. The initial segment is responsible for the first of two

concentration peaks observed in the CMAQ results. However, the initial plume segment has a tangential impact on all stations, leading to smaller concentration increases. The southwesternmost station (Fort McPherson) remains practically unaffected. The larger concentration peaks are caused by the more direct impact from the second plume segment. The plume segmentation observed in the CMAQ simulation is caused by the upper-level bifurcation previously described. Although an interruption in the modeled plume is apparent with CMAQ results, no distinction between smoke plumes from the different prescribed burns is appreciable.

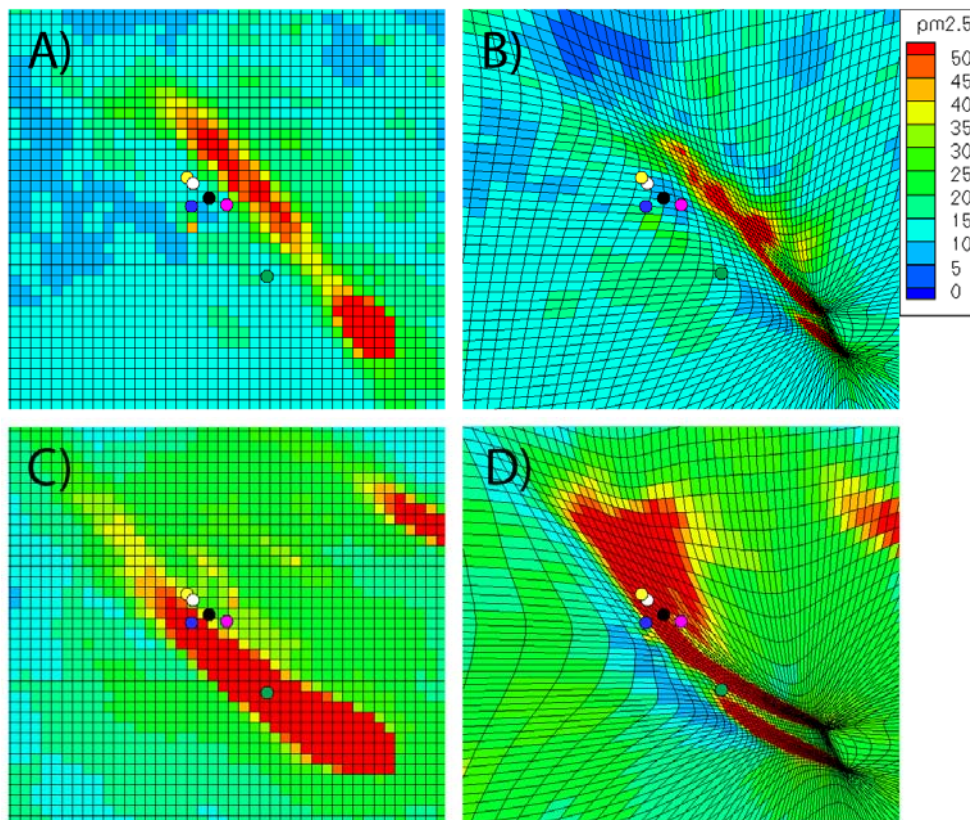


**Figure 5.** Simulated  $PM_{2.5}$  concentrations ( $\mu g m^{-3}$ ) on 28 February 2007 at 22:30 Z using **A)** static grid CMAQ and **B)** AG-CMAQ, and on 1 March at 02:00 Z using **C)** static grid CMAQ and **D)** AG-CMAQ. The locations of the McDonough (green), South DeKalb (pink), Confederate Avenue (black), Fort McPherson (blue), Jefferson Street (white), and Fire Station 8 (yellow) air quality monitoring sites are indicated by the colored circles.

Figure 5b shows surface-level concentrations and monitoring site locations from the AG-CMAQ simulation also at 22:30 Z. From these results no plume segmentation can be observed and plumes from both prescribed burns are clearly distinct. Once again, the earliest impact of the plume at monitoring sites is tangential, and avoids the Fort McPherson site.

Similar plots at 02:00 Z on 1 March for CMAQ and AG-CMAQ simulations are presented in Figures 5c and 5d respectively. The AG-CMAQ simulation indicates that the major modeled concentration peak is attributable to the more northern prescribed burn at Oconee National Forest. This conclusion cannot be derived from the static grid CMAQ results. The southernmost station at McDonough also merits special attention. While nested between plumes in Figure 5d, the site is affected by both plumes at different instances during the AG-CMAQ simulation. This may explain the site's unique double concentration peak recorded in the station measurements. If indeed these observations correspond to distinct hits from different plumes, such behavior can only be deduced with the increased resolution provided by the adaptive grid model, although the initial hit recorded in the measurements at the monitoring site is not perceived from modeled results since the smoke plume is oriented excessively to the east of the site.

### 3.3. Discussion

We believe that differences in simulated concentration fields produced by the static grid and adaptive grid models reflect the improved replication of plume dynamics and decrease in artificial dilution that was achieved through grid refinement. Nevertheless, the consistent under-prediction of maximum  $PM_{2.5}$  concentrations observed from a static grid simulation, although ameliorated, persists throughout the adaptive grid simulation. It is likely that underestimations of fire induced volatile organic compound emissions and secondary organic aerosol formation are largely

responsible for the differences between modeled results and measurements, and that other inputs and processes unrelated to grid resolution contribute significantly to the error in pollutant concentrations. Uncertainties in plume rise, mixing layer height, and prescribed burn emission factors all contribute to model error and should be addressed in an attempt to achieve results more consistent with site measurements.

It is also undeniable that the surface-level concentrations are quite sensitive to wind direction and speed inputs from the meteorological model utilized. The sensitivity to winds becomes even greater when plumes are better defined as in the adaptive grid simulation. Small changes in wind direction can greatly change the impact plumes have on surface-level pollutant concentrations at specified locations. The performance of photochemical models will continue to be constrained by the limitations in fine-scale wind predictions inherent to meteorological models. To address this concern in the future, we plan to apply the grid refinement methodology in AG-CMAQ to meteorological models and develop weather models that can effectively adapt to air pollutant concentrations. Such adaptation will require continuous input of pollutant concentrations from the air quality model into the meteorological model. Therefore, coupled air quality and meteorological adaptive grid models will be created to operate simultaneously at finer scales and continuously exchange feedback.

Finally, the bifurcation observed in the 3D visualization of static grid results may indicate the importance of vertical resolution in achieving better results. Although AG-CMAQ currently provides increased resolution only along the horizontal plane, we plan to extend the grid refinement capability to include the model's vertical layering. This development would allow full grid adaptation of a 3-dimensional domain and may prove to be useful in simulating plume dynamics at even greater levels of detail. Extension of grid adaptation to the third dimension (i.e.,

vertical) would also be extremely useful in resolving cloud processes.

#### 4. Conclusions

An adaptive grid air pollution model (AG-CMAQ) has been developed by integrating a dynamic, solution-adaptive grid algorithm into CMAQ. The model can efficiently refine the grid in response to any defined simulation variable or parameter. Although adaptive grid air pollution models have been previously explored, AG-CMAQ is unique in its capacity to model particulate matter and the first built onto an existing community model. We believe that adaptive grid modeling could potentially be the best approach to multiscale modeling of air pollution dynamics and chemistry.

The developed model was verified and its capabilities were demonstrated. The model proved to replicate results that were practically the same to those produced by the standard, static grid CMAQ when no grid adaptation was applied and effectively increased grid resolution in response to pollutant concentrations increases when adaptation was applied. AG-CMAQ performance was evaluated by simulating an air pollution incident affecting the Atlanta metropolitan area caused by two prescribed burns. The evaluation showed that AG-CMAQ successfully reduced the artificial diffusion inherent to photochemical models and produced better defined plumes compared to the standard CMAQ. Additionally, AG-CMAQ allowed both prescribed burn plumes to be distinctly observed and impacts at specific locations to be attributed to a particular prescribed burn. AG-CMAQ predicted PM<sub>2.5</sub> concentrations with less error than CMAQ at most monitoring station locations affected during the incident. The mean fractional error was reduced by 15% on average, indicating significantly better agreement with site measurements.

The results of this study indicate that AG-CMAQ may provide understanding of air quality and atmospheric dynamics beyond that attainable through a static grid model. However, our evaluation indicates that despite the improvement, AG-CMAQ continues to under-predict PM<sub>2.5</sub> concentrations. It is likely that the error can at least be partially attributed to processes unrelated to grid resolution within the air quality modeling system. Among these, the ability of meteorological models to simulate fine-scale and short-term variability in winds may be of greatest significance.

Adaptive grids are a tool that could prove useful for various applications beyond plume simulation. Grid refinement driven by reactivity may provide insight into atmospheric chemistry. The need for improved fine-scale wind modeling previously mentioned could be addressed by applying an adaptive grid within weather models. Indeed, adaptive mesh modeling is currently being discussed as a tool applicable to climate models to focus on small-scale processes that cannot be resolved in existing models. Some have even suggested that adaptive grid models may provide the only means of resolving these small-scale processes within a single model (Weller et al., 2010). The potential benefits that could be attained through adaptive grid modeling in the field of air pollution photochemical modeling are only briefly explored in this study. However, adaptive grids will likely lead to additional and greater advantages not necessarily restricted to air quality modeling, but encompassing different geophysical models as well.

#### Acknowledgements

This research was supported in part by the U.S. Department of Defense, through the Strategic Environmental Research and Development Program (SERDP) and by the U.S. Department of Agriculture Forest Service through the Joint Fire Science Program (JFSP).

#### References

- Bacon, D.P., Ahmad, N.N., Boybeyi, Z., Dunn, T.J., Hall, M.S., Lee, P.C.S., Sarma, R.A., Turner, M.D., Waight III, K.T., Young, S.H., Zack, J.W., 2000. A dynamically adapting weather and dispersion model: the operational multiscale environment model with grid adaptivity (OMEGA). *Monthly Weather Review* 128, 2044-2076.
- Byun, D., Schere, K.L., 2006. Review of the governing equations, computational algorithms, and other components of the models-3 Community Multiscale Air Quality (CMAQ) modeling system. *Applied Mechanics Reviews* 59, 51-77.
- Coats, C.J., Jr., 1996. High-performance algorithms in the Sparse Matrix Operator Kernel Emissions (SMOKE) modeling system. Preprints, *Ninth Joint Conference on Applications of Air Pollution Meteorology with A&WMA*, Atlanta, GA, American Meteorological Society, 584-588.
- Colella, P., Woodward, P.R., 1984. The piecewise parabolic method (PPM) for gas-dynamical simulations. *Journal of Computational Physics* 54, 174-201.
- Constantinescu, E.M., Sandu, A., Carmichael, G.R., 2008. Modeling atmospheric chemistry and transport with dynamic adaptive resolution. *Computational Geosciences* 12, 133-151.
- Ghorai, S., Tomlin, A.S., Berzins, M., 2000. Resolution of pollutant concentrations in the boundary layer using a fully 3D adaptive gridding technique. *Atmospheric Environment* 34, 2851-2863.
- Hu, Y.T., Odman, M.T., Chang, M.E., Jackson, W., Lee, S., Edgerton, E.S., Baumann, K., Russell, A.G. 2008. Simulation of air quality impacts from prescribed fires on an urban area. *Environmental Science and Technology* 42, 3676-3682.
- Khan, M.N., 2003. *Development and application of an adaptive grid air quality model*. Ph. D. Dissertation, School of Civil & Environmental Engineering, Georgia Institute of Technology, Atlanta, GA, 105-120.
- Khan, M.N., Odman, M.T., Karimi, H.A., 2005. Evaluation of algorithms developed for adaptive grid air quality modeling using surface elevation data. *Computers, Environment and Urban Systems* 29, 718-734.
- Lee, S., Baumann, K., Schauer, J.J., Sheesley, R.J., Naeher, L.P., Meinardi, S., Blake, D.R., Edgerton, E.S., Russell, A.G., Clements, M., 2005. Gaseous and particulate emissions from prescribed burning in Georgia. *Environmental Science and Technology* 39, 9049-9056.
- Liu, Y., Achtemeier, G., Goodrick, S., 2008. Sensitivity of air quality simulation to smoke plume rise. *Journal of Applied Remote Sensing* 2, art. no. 021503.
- MACTEC, 2008. *Documentation of the base G2 and best and final 2002 base year, 2009 and 2018 emission inventories for VISTAS*. Available online from: <http://www.vistas-sesarm.org/documents/VISTABF2003-20-2008.pdf>.
- Michalakes, J., Dudhia, J., Gill, D., Henderson, T., Klemp, J., Skamarock, W., Wang, W., 2005. The weather research and forecast model: software architecture and performance, in *Proceedings of the Eleventh ECMWF Workshop on the Use of High Performance Computing in Meteorology*. Eds. Walter Zwielfhofer and George Mozdzynski, World Scientific, October 25-29, 2004, pp. 156 – 168.
- Odman, M.T., Hu, Y., 2010. A variable time-step algorithm for air quality models. *Atmospheric Pollution Research* 1, 229-238.
- Odman, M.T., Hu, Y., 2007. A variable time-step algorithm for air quality models. *Air Pollution Modeling and its Application XVII: Proceedings of the 27th NATO/CCMS International Technical Meeting on Air Pollution Modelling and Its Application*, held in Banff, Canada, October 24-29, 2004, pp. 411-420 (Eds. Borrego, C., Norman, A.L.), New York, Springer.
- Odman, M.T., Khan, M.N., Srivastava, R.K., McRae, D.S., 2002. Initial application of the adaptive grid air pollution model. *Air Pollution Modeling and its Application XV: Proceedings of the 25th NATO/CCMS International Technical Meeting on Air Pollution Modelling and Its Application*, held in Louvain-la-Neuve, Belgium, October 15-19, 2001, pp. 319-328 (Eds. Borrego, C., Schayes, G.), New York, Kluwer Academic/Plenum Publishers.

- Odman, M.T., Khan M.N., McRae, D.S., 2001. Adaptive grids in air pollution modeling: Towards an operational model, *Air Pollution Modeling and Its Application XIV, Proceedings of the 24th (Millennium) NATO/CCMS International Technical Meeting on Air Pollution Modeling and its Application*, held in Boulder, Colorado, May 15-19, 2000, pp. 541-549, (Eds. Gryning, S.E., Schiermeier, F.A.), New York: Kluwer Academic/Plenum Publishers.
- Sandberg, D.V., Anderson, G.K., Norheim, R.A., 2005. *Fire Emission Production Simulator Tutorial: Student Workbook*. USDA Forest Services, pp. 29-51.
- Smolarkiewicz, P.K., Grell, G.A., 1992. A class of monotone-interpolation schemes. *Journal of Computational Physics* 101, 431-440.
- Srivastava, R.K., McRae, D.S., Odman, M.T., 2001a. Simulation of a reacting pollutant puff using an adaptive grid algorithm. *Journal of Geophysical Research D:Atmospheres* 106, 24245-24257.
- Srivastava, R.K., McRae, D.S., Odman, M.T., 2001b. Simulation of dispersion of a power plant plume using an adaptive grid algorithm. *Atmospheric Environment* 35, 4801-4818.
- Srivastava, R.K., McRae, D.S., Odman, M.T., 2000. An adaptive grid algorithm for air-quality modeling. *Journal of Computational Physics* 165, 437-472.
- Tomlin, A.S., Ghorai, S., Hart, G., Berzins, M., 2000. 3-D Multi-scale air pollution modelling using adaptive unstructured meshes. *Environmental Modelling and Software* 15, 681-692.
- Tomlin, A., Berzins, M., Ware, J., Smith, J., Pilling, M.J., 1997. On the use of adaptive gridding methods for modelling chemical transport from multi-scale sources. *Atmospheric Environment* 31, 2945-2959.
- Weller, H., Ringler, T., Piggott, M., Wood, N., 2010. Challenges facing adaptive mesh modeling of the atmosphere and ocean. *Bulletin of the American Meteorological Society* 91, 105-108.
- Xiao, X., McRae, D.S., Hassan, H.A., Ruggiero, F.H., Jumper, G.Y., 2006. Modeling Atmospheric Optical Turbulence. *44th AIAA-Aerospace Sciences Meeting and Exhibit*, January 9-12, 2006, Reno, Nevada, AIAA-2006-0077.